Initiation of magnetic flux eruptions at accreting black holes

Krzysztof Nalewajko,[a,*] **Mateusz Kapusta**[b] **and Agnieszka Janiuk**[c]

[a]*Nicolaus Copernicus Astronomical Center, Polish Academy of Sciences,*
Bartycka 18, 00-716 Warsaw, Poland

[b]*Warsaw University Observatory,*
Al. Ujazdowskie 4, 00-478 Warszawa, Poland

[c]*Center for Theoretical Physics, Polish Academy of Sciences,*
Al. Lotnikow 32/46, 02-668 Warsaw, Poland

E-mail: knalew@camk.edu.pl

Black holes (BH) acquire relativistic magnetospheres by accreting magnetized gas. Once they collect significant magnetic flux across the horizon, aided by the spin they can drive powerful relativistic jets by the Blandford-Znajek mechanism. Large enough BH magnetic flux backreacts on the accretion flow, which has been described in terms of arresting or choking. Magnetic flux eruptions have been identified as the mechanism of BH magnetic flux saturation. These eruptions can potentially dissipate a large fraction of magnetic energy in the BH magnetosphere by means of relativistic magnetic reconnection, accelerating particles and producing flares of non-thermal radiation. We analyze the results of 3D general-relativistic ideal magnetohydrodynamic (GRMHD) numerical simulations of accretion flows onto magnetically saturated Kerr BHs, focusing on the initiation of magnetic flux eruptions.

---

*Speaker

1. Introduction

Accretion flow onto a BH may advect poloidal magnetic field that accumulates across the BH horizon (with magnetic flux Φ_{BH}), forming a relativistic magnetosphere. Such magnetosphere on a spinning BH (with spin parameter $a > 0$ of the Kerr metric) drives an outflowing Poynting flux $S \propto f(a)\,\Phi_{BH}^2$ [2] (with $f(a) \simeq a^2$ for $a < 0.3$, steepening for $a > 0.3$; [16]) that over large distances accelerates and collimates into a powerful relativistic jet, such as observed in many active galactic nuclei (AGN; in particular radio galaxies and blazars), X-ray binaries, gamma-ray bursts, etc. The amount of magnetic flux that can be accumulated on a BH is limited to $\Phi_{BH,max} \simeq 50\dot{M}^{1/2}$ (in natural Gaussian units with $c = G = M = 1$; with $\dot{M}$ the mass accretion rate) by a saturation mechanism, in which excess magnetic flux appears to be spontaneously ejected in magnetic flux eruptions [16].

Such a magnetically saturated accretion state has been described by [16] as the Magnetically Arrested Disk (MAD), referring to the model of [11]; or alternatively as the Magnetically Choked Accretion Flow [9]. The arresting effect means that strong 'vertical' field (latitudinal component B^θ) forms a direct barrier to the accretion flow, and the choking effect means latitudinal (along θ) compression of the accretion flow by bulging magnetospheres dominated by twisted split monopole (mainly radial component B^r with weaker toroidal component B^ϕ). A magnetically arrested accretion flow could proceed further by means of interchange (magnetic Rayleigh-Taylor) instability, which should develop a strong azimuthal (along ϕ) structure. Interchange instability has been demonstrated within the tubes of vertical magnetic field, ejected by BH flux eruptions, that locally arrest the outer accretion flow [19]. However, GRMHD simulations of magnetically saturated BH accretion states show that $|B^\theta| \ll |B^r|$ (the dominant component is split monopole, rather than vertical), i.e., the magnetic flux through the equatorial plane $\Phi_{eq} \ll \Phi_{BH}$ [1]. Moreover, radial profiles of gas density (averaged over t, θ, ϕ) are consistent with a power law $\rho \propto r^{-1}$ [1]. Our own simulations show that accretion flows in a saturated state between magnetic flux eruptions appear smooth and stable, without signs of interchange instability. This indicates that in a magnetically saturated state accretion flows are not arrested or choked. We suggest that the bulging magnetospheres merely constrict the innermost accretion flows into geometrically thin disks. Recognizing the key role of the rigid structure (slowly rotating and firmly elevated) of horizon-disconnected magnetic field lines anchored along the equatorial current layer, we propose to describe them as *magnetically channeled* [6].

Recently, BH magnetic flux eruptions have been investigated by means of 'extremely high resolution' 3D ideal GRMHD simulations, demonstrating that eruptions are driven by the relativistic magnetic reconnection [13]. This finding is consistent with the dominance of split monopole magnetic fields. Previous simulations at lower resolutions could not achieve sufficiently thin current layers (high Lundquist numbers) that due to tearing instability would break into magnetic flux tubes (plasmoids), maintaining reconnection in the fast regime with reconnection rate independent of numerical magnetic diffusion. However, low-resolution simulations can capture the overall dynamics of BH flux eruptions. A number of issues remain to be explained, including the triggering mechanism for eruptions (e.g., does it involve particular magnetic field configurations?), or the transition of dense accretion flow into an outflowing current layer.

We began to investigate the mechanism of BH magnetic flux eruptions by analyzing 3D

GRMHD simulations with a 'standard resolution' of $N_r = 288$, $N_\theta = N_\phi = 256$, presented in [8]. Finding those results quite complicated, we decided to check whether magnetic saturation and flux eruptions can be studied at a much lower resolution. Surprisingly, most of the features of magnetic flux eruptions can be captured at a 'very low resolution' of $N_r = 72$, $N_\theta = N_\phi = 64$. We find it illustrative to present such a demonstration here. We have carefully compared these very low resolution results with the results obtained at standard resolution that will be presented elsewhere.

2. Setup of GRMHD simulations

We performed 3D numerical simulations of magnetized accretion onto Kerr BHs with spins $|a| = 0, 0.9$, using the ideal GRMHD public code `Athena++` [15, 18]. Simulation was performed in the horizon-penetrating quasi-spherical Kerr-Schild coordinates $r_{\min} \leq r \leq 200$ (for $r_{\min}$ values see Table 1), $0 \leq \theta \leq 180°$, $0 \leq \phi < 360°$ at effective resolution of $N_r = 72$, $N_\theta = N_\phi = 64$, using 1 level of static mesh refinement. Each simulation was initiated from an axisymmetric torus in hydrodynamic equilibrium described by [7]. For $|a| = 0.9$, two simulations were performed for either prograde (reference $a = 0.9$ case) or retrograde (denoted as $a = -0.9$) torus. The tori were set to extend from $r_{\text{in}} = 6$ to $r_{\text{out}} \simeq 70$, with the maxima of density $\rho_{\text{peak}} = 1$ and pressure P_{peak} at r_{peak} (Table 1). The magnetic vector potential was set as $A_\phi \propto r^5 \max\{\rho - \rho_{\max}/20, 0\}$, peaking at $r_{\text{peak,A}}$ (Table 1), and normalized so that at r_{peak} the magnetic enthalpy density is b^2_{peak} and the plasma parameter is $\beta_{\text{peak}} = 2P_{\text{peak}}/b^2_{\text{peak}}$ (Table 1). We adopted the adiabatic index of $\gamma = 13/9$, floor profiles of density $\rho_{\text{floor}}(r) = \max\{10^{-4}r^{-1.5}, 10^{-6}\}$ and pressure $P_{\text{floor}}(r) = \max\{10^{-6}r^{-2.5}, 10^{-8}\}$, and limits on the plasma parameter $\beta_{\min} = 10^{-3}$, magnetization $\sigma_{\max} = 100$ and bulk Lorentz factor $u^t_{\max} = 50$.

Table 1: Parameters of the initial torus configuration for different spin values.

a	$r_{\min}$	r_{peak}	$r_{\text{peak,A}}$	P_{peak}	b^2_{peak}	β_{peak}
0.9	1.074	13.00	34	0.0066	6.9×10^{-6}	1920
0	1.753	15.91	37	0.0046	5.0×10^{-6}	1860
-0.9	1.074	22.20	44	0.0026	4.5×10^{-6}	1150

3. Analysis of a magnetic flux eruption

Figure 1 presents short term evolution of Φ_{BH} during the magnetic flux eruption starting at $t \simeq 15200$. The BH magnetic flux decreases by 25% over the period of $\Delta t \sim 250$. We also present maps of mass density ρ, temperature $T = P/\rho$ (P is the pressure) and radial velocity v^r projected onto the (r, ϕ) plane. In order to encompass the entire accretion flow, for each value of (r, ϕ) we show a suitable parameter statistic over a broad range of θ. The magnetic flux eruption can be seen as (1) density gap, (2) relativistic temperature, (3) radial outflow. The eruption is limited to a narrow sector of azimuth ϕ and anchored to the BH horizon (rather than the ergosphere boundary). Over time, it expands radially (Section 3.2) and rotates prograde (counterclockwise in this case) around the BH axis at steady rates (Section 3.3). In particular, the highest temperature is located along the leading edge of the density gap.
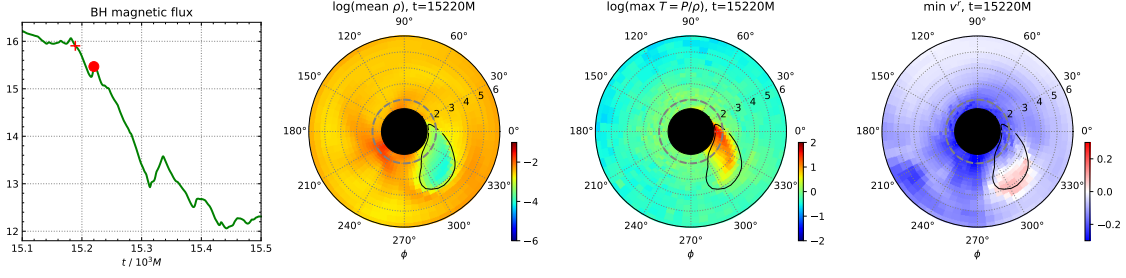
3

Figure 1: Magnetic flux eruption developing in a sector of prograde accretion flow for $a = 0.9$. First panel from the left: magnetic flux across the BH horizon as function of simulation time (the red circle indicates the moment presented in other panels; the red cross indicates an earlier moment presented in Figure 3). The other panels show maps of the accretion flow in the Kerr-Schild coordinates (r, ϕ) projected onto the equatorial plane $\theta = 90°$ by taking a statistic over $45° < \theta < 135°$. Second panel: mean density (log scale); third panel: maximum temperature (log scale); fourth panel: radial velocity v^r. The black line is a contour of density $\log \rho_{\text{mean}} = -3$. The black circle indicates the BH outer horizon, and the gray dashed line the ergosphere boundary.
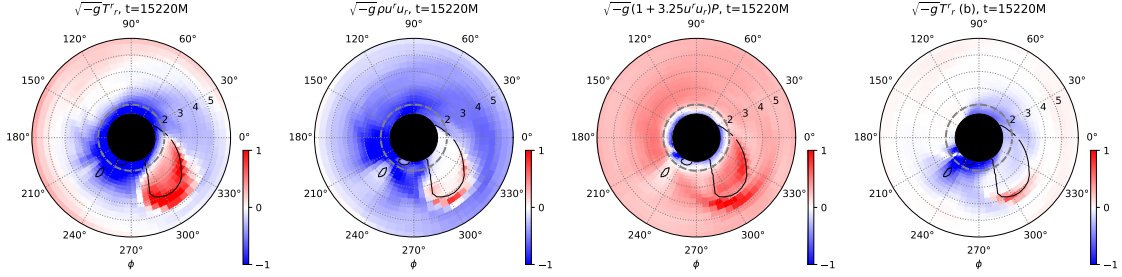

Figure 2: Maps in the (r, ϕ) coordinates along the equatorial plane ($\theta \simeq 90°$) showing decomposition of the radial stress tensor $T^r{}_r$ scaled by $\sqrt{-g}$. From the left, the panels show: (1) total $T^r{}_r$; (2) contribution of plasma inertia; (3) contribution of plasma enthalpy; (4) contribution of magnetic fields. All components are shown in the same color scale (blue - negative, white - zero, red - positive) in the same arbitrary units.

3.1 The driver of radial outflow

In order to determine the driving mechanism for the radial outflow in magnetic flux eruption, Figure 2 presents decomposition of the radial stress tensor $T^r{}_r$, the radial gradient of which is the most important contribution in the conservation of radial momentum $\partial_\mu \left(\sqrt{-g} T^\mu{}_r \right) = \sqrt{-g} \Gamma^\sigma{}_{\rho r} T^\rho{}_\sigma$. The radial stress tensor is decomposed into contributions from plasma inertia $\rho u^r u_r$, plasma enthalpy $((13/4) u^r u_r + 1) P$, and magnetic fields $b^2 u^r u_r + b^2/2 - b^r b_r$. The regular accretion flow is characterized by a virial balance in $T^r{}_r$ between negative contribution of plasma inertia and positive contribution of plasma enthalpy. In contrast, the magnetic flux eruption is characterized by strong positive excess of $T^r{}_r$, which results mainly from a gap in the contribution of plasma inertia. The contribution of plasma enthalpy shows localized excesses along the leading azimuthal edge of the eruption (possibly due to most active reconnection) and outside the radial edge (possibly due to a shock in the accretion flow). The contribution of magnetic fields is not important.

3.2 3D renderings of magnetic field lines

Figure 3 shows 3D renderings of selected complete samples of magnetic field lines at two stages in development of the flux eruption ($t = 15189M, 15220M$). Those field lines were integrated in the Kerr-Schild coordinates (r, θ, ϕ) from magnetic 3-vectors B^i using a 4th order Runge-Kutta scheme. We highlight magnetic connections by distinguishing lines connected to (blue) and disconnected from (green) the BH horizon. The lines were seeded from fixed positions: just under the horizon ($r = 1.4$) for the connected lines, or at $r = 5.5$ for the disconnected lines (requiring that $r_{\rm H} < r_{\rm line,min} < 4$; $r_{\rm H} = 1 + \sqrt{1 - a^2}$ is the BH outer horizon). Only two layers of connected field lines are shown, seeded at the cells adjacent to the equatorial plane $\theta = 90°$. In addition, we show transparent surface contours for gas density ($\log_{10} \rho = -3$; showing the density gap) and relativistic temperature ($\log_{10} T = 0.5$; showing the region of active reconnection) (cf. Fig. 1).

In the advanced stage of the eruption ($t = 15220M$), a thin 'tongue' of relativistic temperature partially fills the density gap. Horizon-connected magnetic field lines are partially immersed in the tongue. Horizon-disconnected field lines are also present within the tongue, but only in its outer part. Thus, horizon-connected field lines can meet directly with anti-parallel orientation, which is optimal for magnetic reconnection with very weak guide field [17]. A pile-up of disconnected field lines can be seen along the outer edge of the density gap, with horizon connected lines bulging above.

In the early stage of the eruption ($t = 15189M$), both the density gap and the reconnection tongue are much smaller, and their footpoint is shifted clockwise, which is consistent (noting that this is an earlier time step) with prograde rotation of the footpoint around the BH spin axis (Section 3.3). We also show that the spiral arms of the horizon-disconnected field lines passing through that density gap are characterized by very high magnetization ($\log_{10} \sigma > 1$) and radial outflow ($v^r > 0.1$). Being also the most elevated from the equatorial plane, those lines are consistent with an azimuthally localized wind.

Apart from the localized eruption, the accretion flow is smooth, showing no signs of instabilities like interchange. In the high density regions, horizon-connected field lines are separated by the disconnected lines forming regular, gently spiral loops, apparently stretched by the plunging ($v^r \lesssim -0.2$) accretion flow. Magnetization shows strong latitudinal (along θ) stratification with the inner tips of the disconnected lines dominated by plasma enthalpy ($\log_{10} \sigma < -1$), and their spiral arms roughly in equipartition ($\log_{10} \sigma \sim 0$). This reflects mainly the θ-stratification of plasma density ρ, since the magnetic field enthalpy density b^2 is roughly uniform (except for a narrow equatorial current layer).

3.3 Rotation of the eruption footpoint

Figure 4 presents spacetime diagrams in the (ϕ, t) coordinates of plasma temperature measured at $r \simeq 2.5M$ for three simulations with different BH spins $a = 0.9, 0, -0.9$. The footpoints of individual magnetic flux eruptions, seen as patches of relativistic temperature ($\log T_{\rm max} > 1$), rotate systematically. We identify the rotation period of $P \simeq 170M$ as roughly consistent (this is not a fit) with the evolution of some eruptions for every considered spin value (in the retrograde case of $a = -0.9$ the strongest eruption rotates significantly faster with $P \simeq 65M$).
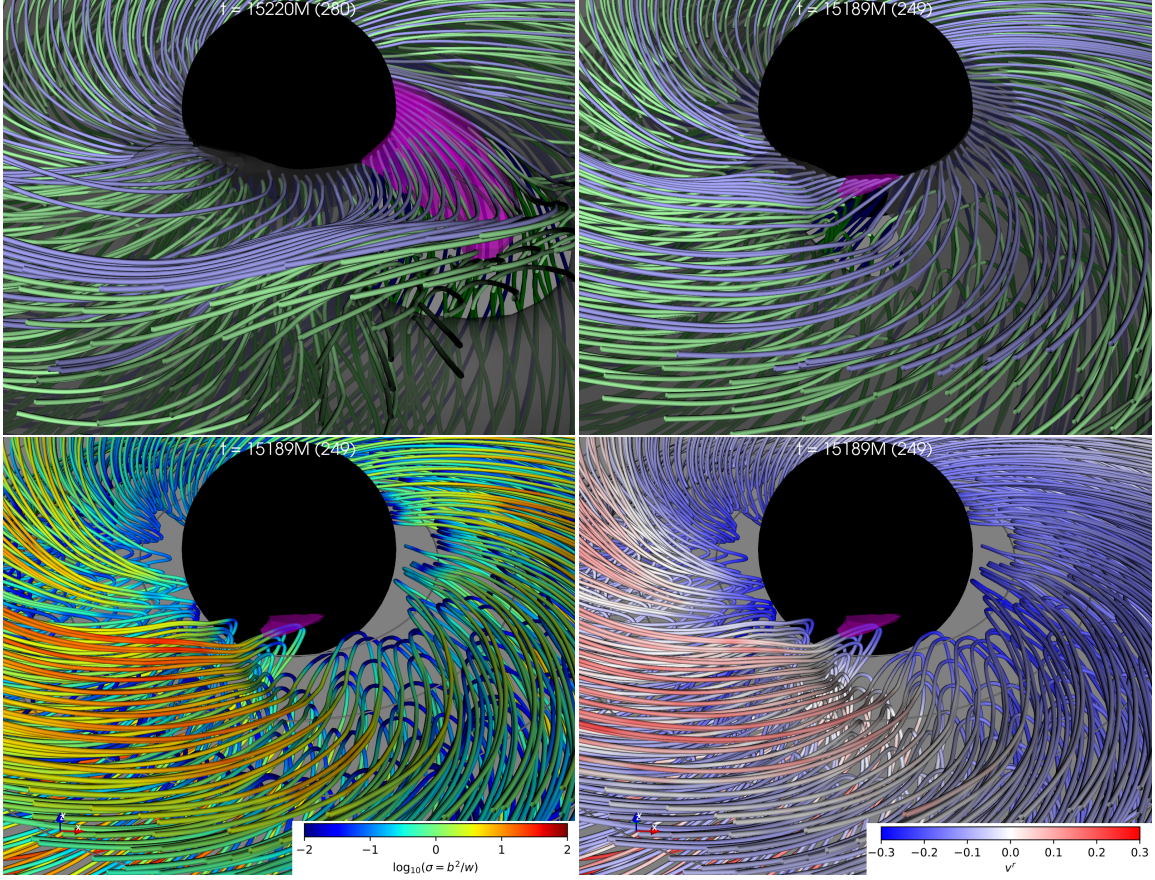
Figure 3: 3D renderings (in Kerr-Schild coordinates represented as ordinary spherical; seen at inclination angle 45° from the equatorial plane) of selected magnetic field lines for two moments during the evolution of magnetic flux eruption indicated in Figure 1. In the upper row of panels, the blue lines show magnetic field lines connected to the BH horizon (the black sphere) near the equatorial plane (a complete sample seeded at $r = 1.4$ for every cell in ϕ and two nearest cells in θ); the green lines show magnetic field lines disconnected from the BH horizon (a complete sample seeded at $r = 5.5$ with $r_{\mathrm{H}} < r_{\mathrm{min}} < 4$ for every cell in ϕ and $45° < \theta < 90°$); light line colors indicate that $B^r > 0$, and dark line colors indicate $B^r < 0$; the magenta surfaces indicate reconnection regions with relativistic temperature $\log_{10} T > 0.5$; the gray surfaces indicate accretion flow regions with high density $\log_{10} \rho > -3$. In the lower row of panels, only disconnected field lines are shown (density contour is not shown): in the lower left panel they are colored by the magnetization $\sigma = b^2/w$; in the lower right panel they are colored by the radial 3-velocity v^r. Density of the lines does not represent the magnetic field strength.

4. Discussion

This preliminary analysis demonstrates that key features of magnetic flux saturation and eruptions can be reproduced by ideal GRMHD simulations of very low resolution. The features demonstrated here are: saturation level of normalized BH magnetic flux $\Phi_{\mathrm{BH}}/\dot{M}^{1/2} \sim 50$, large relative amplitude of Φ_{BH} decrease ($\sim 25\%$), smooth magnetically constricted accretion flow (known to be sub-Keplerian, with much of its angular momentum removed by laminar winds; [14]), self-similar evolution of the eruption region defined by (1) density gap, (2) relativistic temperature, (3) radial
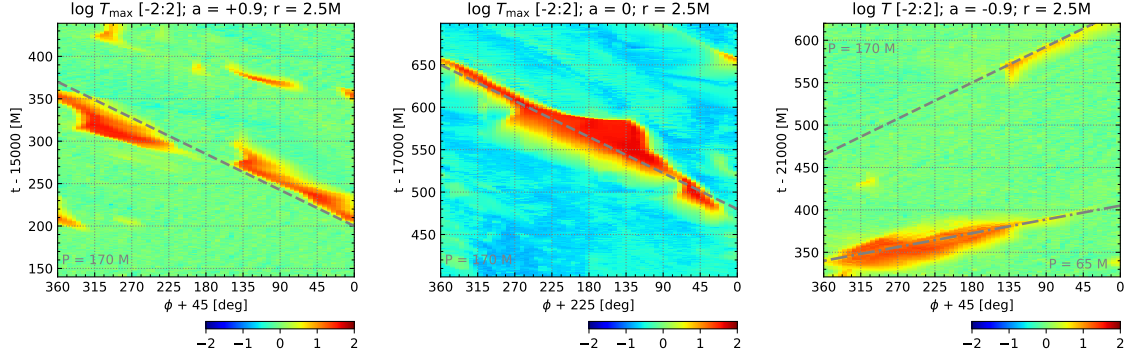
Figure 4: Spacetime diagrams in the (ϕ, t) coordinates of maximum plasma temperature T_{max} over latitudinal range $45° < \theta < 135°$ at fixed $r \simeq 2.5M$, compared for three simulations with BH spin values $a = +0.9$ (prograde; left panel), $a = 0$ (middle panel), $a = -0.9$ (retrograde; right panel). Dashed lines indicate trends of linear rotation with the period of $P = 170M$. Dash-dotted line in the right panel indicates a trend of linear rotation with the period of $P = 65M$.

outflow. Further evolution of this simulation also shows that the ejected magnetic flux tube forms an orbiting 'hotspot', similar to those investigated by, e.g., [4, 12] in the context of infrared flares of Sgr A* resolved astrometrically by VLTI/GRAVITY.

The trigger of relativistic reconnection in such magnetically saturated state does not seem to involve unusual magnetic field line configurations. The self-similar evolution of the eruption suggests a positive feedback loop in the equatorial current layer: decreasing density leads to stronger heating by reconnection, which leads to pressure build-up, which drives the radial outflow, which leads to further decrease of density. As the accreting BH becomes saturated with magnetic flux, the accretion flow (a magnetic insulator with inactive current layer) is geometrically constricted to a critically thin level, in which a minor localized density fluctuation may initiate the feedback loop (puncture the insulator and activate the current layer). This suggests that a magnetically saturated accreting BH may be in the state of self-organized criticality, which would predict that energies released by individual eruptions should follow a power-law distribution $N(E) \propto E^{-\alpha}$ with $\alpha \simeq 1.5$ (depending on effective dimension) [e.g., 5]. Activation of pre-existing current layer by thinning plasma represents a novel scenario for triggering relativistic magnetic reconnection, which would be worth exploring in the kinetic regime.

Highly sub-Keplerian and spin-independent rotation periods ($\simeq 1.2°/M$, corresponding to $\simeq 300M$) of patterns in the lensed ring images of magnetically saturated accreting BHs have been obtained by ray tracing results of 3D GRMHD simulations [3]. Such periods are comparable with the possible rotation rate of the M87* image and total linear polarization, $\simeq 3.9°/$day corresponding to $\simeq 250M$ [10]. The rotation of magnetic flux eruption footpoints cannot be explained in terms of patterns, since magnetic reconnection is a physical process and reconnection regions connect to particular mass-loaded magnetic field lines. Spin-independent rotation rates at $r \sim 2.5M$ can be explained by the rigidity of horizon-disconnected magnetic field lines that channel regular plunging accretion flow through converging nozzle constricted by bulging BH magnetosphere.

References

[1] Begelman, M. C., Scepi, N., & Dexter, J. 2022, *MNRAS*, 511, 2040

[2] Blandford, R. D. & Znajek, R. L. 1977, *MNRAS*, 179, 433

[3] Conroy, N. S., Bauböck, M., Dhruv, V., et al. 2023, *ApJ*, 951, 46

[4] Dexter, J., Tchekhovskoy, A., Jiménez-Rosales, A., et al. 2020, *MNRAS*, 497, 4999

[5] Feinstein, A. D., Seligman, D. Z., Günther, M. N., et al. 2022, *ApJ*, 925, L9

[6] Ferreira, J. & Pelletier, G. 1993, *A&A*, 276, 637

[7] Fishbone, L. G. & Moncrief, V. 1976, *ApJ*, 207, 962

[8] Janiuk, A. & James, B. 2022, *A&A*, 668, A66

[9] McKinney, J. C., Tchekhovskoy, A., & Blandford, R. D. 2012, *MNRAS*, 423, 3083

[10] Nalewajko, K. 2023, *The Sixteenth Marcel Grossmann Meeting*, 339

[11] Narayan, R., Igumenshchev, I. V., & Abramowicz, M. A. 2003, *PASJ*, 55, L69

[12] Porth, O., Mizuno, Y., Younsi, Z., et al. 2021, *MNRAS*, 502, 2023

[13] Ripperda, B., Liska, M., Chatterjee, K., et al. 2022, *ApJ*, 924, L32

[14] Scepi, N., Begelman, M. C., & Dexter, J. 2024, *MNRAS*, 527, 1424

[15] Stone, J. M., Tomida, K., White, C. J., et al. 2020, *ApJS*, 249, 4

[16] Tchekhovskoy, A., Narayan, R., & McKinney, J. C. 2011, *MNRAS*, 418, L79

[17] Werner, G. R. & Uzdensky, D. A. 2017, *ApJ*, 843, L27

[18] White, C. J., Stone, J. M., & Gammie, C. F. 2016, *ApJS*, 225, 22

[19] Zhdankin, V., Ripperda, B., & Philippov, A. A. 2023, *PhRvR*, 5, 043023

PoS(HEPROVII)041